# Preparation and pharmacological characterization of the enantiomers of the anticancer agent R/S-N-3-cyanophenyl-N'-(6-tert-butoxycarbonylamino-3,4-dihydro-2,2-dimethyl-2H-1-benzopyran-4-yl)urea

Schnekenburger, Michael; Goffin, Eric; Schoumacher, Matthieu; Tumanov, Nikolay; Mouithys-Mickalad, Ange; de Tullio, Pascal; Wouters, Johan; Lebrun, Philippe; Diederich, Marc; Pirotte, Bernard

*Published in:*
European Journal of Medicinal Chemistry Reports

*DOI:*
10.1016/j.ejmcr.2024.100244

*Publication date:*
2025

*Document Version*
Publisher's PDF, also known as Version of record

European Journal of Medicinal Chemistry Reports 13 (2025) 100244

Contents lists available at ScienceDirect

European Journal of Medicinal Chemistry Reports

journal homepage: www.editorialmanager.com/ejmcr/default.aspx

# Preparation and pharmacological characterization of the enantiomers of the anticancer agent *R/S-N*-3-cyanophenyl-*N'*-(6-tert-butoxycarbonylamino-3,4-dihydro-2,2-dimethyl-2*H*-1-benzopyran-4-yl)urea: Identification of the *R*-enantiomer as the active eutomer

Michael Schnekenburger [a], Eric Goffin [b], Matthieu Schoumacher [b], Nikolay Tumanov [c], Ange Mouithys-Mickalad [d], Pascal de Tullio [b], Johan Wouters [c], Philippe Lebrun [e], Marc Diederich [f,**,1], Bernard Pirotte [b,*,1]

[a] *Laboratoire de Biologie Moléculaire et Cellulaire Du Cancer, Fondation de Recherche Cancer et Sang, BAM 3, Pavillon 2, 6A Rue Nicolas-Ernest Barblé, L-1210, Luxembourg*
[b] *Laboratoire de Chimie Pharmaceutique, Center for Interdisciplinary Research on Medicines (CIRM), Université de Liège, Quartier Hôpital, Avenue Hippocrate 15, B-4000, Liège, Belgium*
[c] *Département de Chimie, Université de Namur, 61, Rue de Bruxelles, B-5000, Namur, Belgium*
[d] *Centre for Oxygen, Research & Development (CORD)-CIRM, Institut de Chimie, Université de Liège, Allée de La Chimie, 3, 4000, Liège, Belgium*
[e] *Laboratoire de Physiologie et Pharmacologie, Université Libre de Bruxelles, Faculté de Médecine, 808 Route de Lennik, B-1070, Bruxelles, Belgium*
[f] *Department of Pharmacy, Research Institute of Pharmaceutical Sciences & Natural Products Research Institute, College of Pharmacy, Seoul National University, 1, Gwanak-Ro, Gwanak-Gu, Seoul, 08826, Republic of Korea*

ARTICLE INFO

*Keywords:*
2,2-Dimethylchromans
Racemate
Enantiomeric separation
Pancreatic B-Cell
Potassium channel opener
Anticancer agent
Glucose metabolism
Sirtuin inhibitor
Leukemia

ABSTRACT

R/S-N-3-cyanophenyl-N'-(6-tert-butoxycarbonylamino-3,4-dihydro-2,2-dimethyl-2*H*-1-benzopyran-4-yl)urea (BPDZ 711, **4**) initially designed as a $K_{ATP}$ channel opener, was found to exhibit diverse biological activities. The compound inhibited insulin release from rat pancreatic islets, indicating a potential effect on glucose metabolism. Oxygraphy measurements on chronic myeloid leukemia (CML) K-562 cells revealed an impact on cellular respiration. Additionally, the compound demonstrated inhibitory activity on histone deacetylase class III enzymes (sirtuins), linking metabolic and epigenetic regulation. This was corroborated by its effect on protein acetylation and modulation of the extracellular pH of treated CML cells. Alterations in CML cells' nuclear morphology and the release of high-mobility group box 1 (HMGB1) protein confirmed mechanisms related to cellular stress and immunogenic cell death. BPDZ 711 preserved the viability of peripheral blood mononuclear cells, thus demonstrating excellent differential toxicity.

Since BPDZ 711 is a racemate, the present study focused on the preparation of the two enantiomers and examined the possibility that each isomer could display a distinct pharmacological profile. Our data revealed that the R-enantiomer (**5**) of BPDZ 711 was consistently the most biologically active compound (eutomer), making it the reference compound for future drug discovery and development.

## 1. Introduction

Among the 2,2-dimethylchromans studied as ATP-sensitive potassium ($K_{ATP}$) channel openers (PCOs) which are structurally related to the reference cromakalim (**1**), diversely 6-substituted 4-phenylureido/4-phenylthioureido-2,2-dimethylchromans exerted a potent inhibitory activity on insulin-secreting cells due to the activation of the pancreatic SUR1-type $K_{ATP}$ channels [1–4]. Unlike cromakalim, which

* Corresponding author.
** Corresponding author.
*E-mail address:* b.pirotte@uliege.be (B. Pirotte).
[1] (equal contribution).

https://doi.org/10.1016/j.ejmcr.2024.100244
Received 26 October 2024; Received in revised form 17 December 2024; Accepted 18 December 2024
Available online 19 December 2024

preferentially activates the vascular smooth muscle SUR2B-type $K_{ATP}$ channels, a significant selectivity for the pancreatic versus the vascular smooth muscle tissue was observed with several 4-phenylureido/4-phenylthioureido-2,2-dimethylchromans (*i.e.*, compounds **2** and **3**; Fig. 1) [1].

Surprisingly, enhanced activity on pancreatic β-cells was observed with a series of 4-phenylureido-substituted 2,2-dimethylchromans bearing a bulky alkoxycarbonylamino group at the 6-position of the chroman ring. The 6-tert-butoxycarbonylamino-substituted compound (**4**) [*R/S-N*-3-cyanophenyl-N'-(6-tert-butoxycarbonylamino-3,4-dihydro-2,2-dimethyl-2*H*-1-benzopyran-4-yl)urea or BPDZ 711 (**4**)] was the most potent inhibitor of glucose-induced insulin release; with an inhibitory concentration $IC_{50}$ of 0.24 μM. At high concentrations, the $K_{ATP}$ channel opener BPDZ 711 (**4**) also acted as a calcium entry blocker and promoted intracellular calcium translocation [5].

6-halo-substituted- and 6-alkoxycarbonylamino-substituted 2,2-dimethylchromans bearing an arylurea or arylthiourea moiety at the 4-position were also described as potent inhibitors of glioma cell proliferation [6]. Among these antiproliferative agents, BPDZ 711 (**4**) potently inhibited histone deacetylase (HDAC) class III sirtuins 1 and 2 (SIRT1/2) activities associated with marked antiproliferative activity on glioblastoma cells while having little impact on normal glial cells, thus demonstrating excellent differential toxicity. Moreover, the anticancer potential of BPDZ 711 (**4**) was also confirmed in 3D glioblastoma spheroids and by zebrafish xenografts *in vivo* [7].

Given the potential interaction of potassium channel openers with mitochondrial $K_{ATP}$ channels, we further characterized the effects of BPDZ 711 (**4**) on mitochondrial respiratory parameters in cardiomyocytes and its effects on calcium homeostasis in isolated mouse liver mitochondria [8]. We concluded that the compound behaved, at least, as a potent reversible inhibitor of the mitochondrial electron transport chain.

Previous research explored new targets for eradicting persistent chronic myeloid leukemia (CML) stem cells. Transcriptomic data from healthy individuals and CML patients led to the development of a disease-specific network focusing on SIRT1/2, which regulates metabolism and cell survival. The therapeutic potential of SIRT1/2 inhibition was assessed using siRNA and BPDZ 711 (**4**, referred to as Si-711 in Ref. [9]) in imatinib-sensitive and -resistant CML cell lines. SIRT1/2 inhibition by BPDZ 711 disrupted key transcription factors like Myc, reduced oxidative phosphorylation, and caused energy depletion, leading to regulated necrosis. Combining BPDZ 711 (**4**) with imatinib significantly enhanced anti-CML effects *in vitro* and *in vivo*. Notably, BPDZ 711 (**4**) induced the release of damage-associated molecular patterns, enhanced phagocytosis, promoted immunogenic cell death, and allowed us to explore a pre-clinical anti-CML vaccination approach [9].

Consequently, BPDZ 711 (**4**) exhibits a promising multitarget profile and potential as an anticancer agent for glioblastoma and leukemia. Since the compound is a racemate, the aim of this work was to separate the two enantiomers [Fig. 2; R-BPDZ 711 (or BPDZ 811, **5**) and S-BPDZ 711 (or BPDZ 812, **6**)] and investigate whether each isomer could express a distinct pharmacological profile. This information is critical for the development of new anticancer drugs belonging to this class of compounds.

## 2. Results and discussion

### 2.1. Chemistry

#### 2.1.1. Synthesis and enantiomeric separation

The synthesis of the two enantiomers of BPDZ 711 (**4**) is described in Scheme 1. The starting compound **7** was obtained as previously described [4]. Preparative chromatographic purification on the chiral column Chiralcel OD-H was performed to separate the two enantiomers (Fig. 3). The first eluted enantiomer was characterized as the R-isomer **8** by examining its S-naproxen salt **10** by X-ray crystallography (Fig. 4). The two separated enantiomers of **7** were then converted into their respective *N*-aryl-*N'*-alkyl-substituted urea compounds **5** (R-BPDZ 711 or BPDZ 811) and **6** (S-BPDZ 711 or BPDZ 812) after reaction with 3-cyanophenyl isocyanate.

Moreover, the two separated isomers of BPDZ 711 (**4**) were also obtained in larger amounts from the racemate by preparative chromatographic purification on the chiral column Chiralcel OD-H (Fig. 5) and individually characterized by comparison with authentic samples of each enantiomer obtained in accordance with the pathway reported in Scheme 1.

#### 2.1.2. Conformational study

BPDZ 711 (**4**) belongs to the *N,N'*-disubstituted urea derivatives known to exist in different conformations in solution and in the solid state [10–16]. Ureas and thioureas bearing an alkyl and/or an aryl substituent on the nitrogen atoms are expected to adopt four preferential low-energy conformations assuming an optimal electron delocalization in the planar urea/thiourea system (see Fig. 6; X = O for ureas; X = S for thioureas, conformations A, B, C, and D). Conformation A with two N-H groups in a parallel orientation is the most common [10,13]. Additionally, ureas and thioureas can adopt different tautomeric forms [Fig. 6: X = O, urea (A)/uronium (A′, A″) forms; X = S, thiourea (A)/thiouronium (A′, A″) forms] in solution and in the solid state. As a result, the question arose as to whether BPDZ 711 (**4**), despite existing as two distinct enantiomers, might adopt different stable conformations or tautomeric forms in a biological medium that could interact differently with its various targets.

We attempted to determine the conformation/tautomeric form adopted by BPDZ 711 (**4**) in the solid state (X-ray crystal structure analysis) and in solution (NMR NOESY and $^{15}N$-$^{1}H$ HSQC experiments in DMSO-$d_6$). However, we were unable to obtain suitable crystals of BPDZ 711 (**4**) for determining its solid-state conformation via X-ray diffraction (the compound crystallized in fine needles). Nonetheless, we obtained appropriate crystals of BPDZ 645 (**11**, Fig. 7), the 6-methoxycarbonyl amino-substituted analog of BPDZ 711 (**4**). In the solid state, compound **11** adopted conformation A (Fig. 6), supporting that the structurally related BPDZ 711 (**4**) could adopt the same conformation.

NMR experiments were conducted on BPDZ 711 (**4**) in DMSO-$d_6$, as well as on its thiourea counterpart, BPDZ 625 (**12**) (Fig. 8A). The $^{15}N$-$^{1}H$ HSQC spectrum of BPDZ 711 (**4**) (Fig. 8B) and compound **12** (Fig. 8C) showed that the hydrogen atoms are linked to the nitrogen atoms of the urea [NH(**2**) and NH(**3**)] and the thiourea [NH(**1**) and NH(**3**)] functions; this observation theoretically excludes the (thio)uronium tautomeric

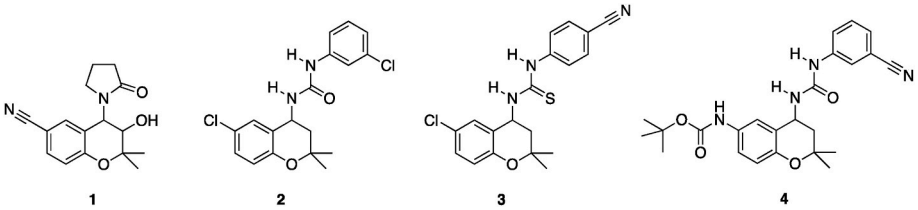


**Fig. 1.** Structure of the SUR2B-type $K_{ATP}$ channel opener cromakalim (**1**) and diversely 6-substituted 4-phenylureido/4-phenylthioureido-2,2-dimethylchromans [**2**, **3** and **4** (BPDZ 711)] reported as activators of pancreatic SUR1-type $K_{ATP}$ channels and subsequently inhibitors of insulin-release.

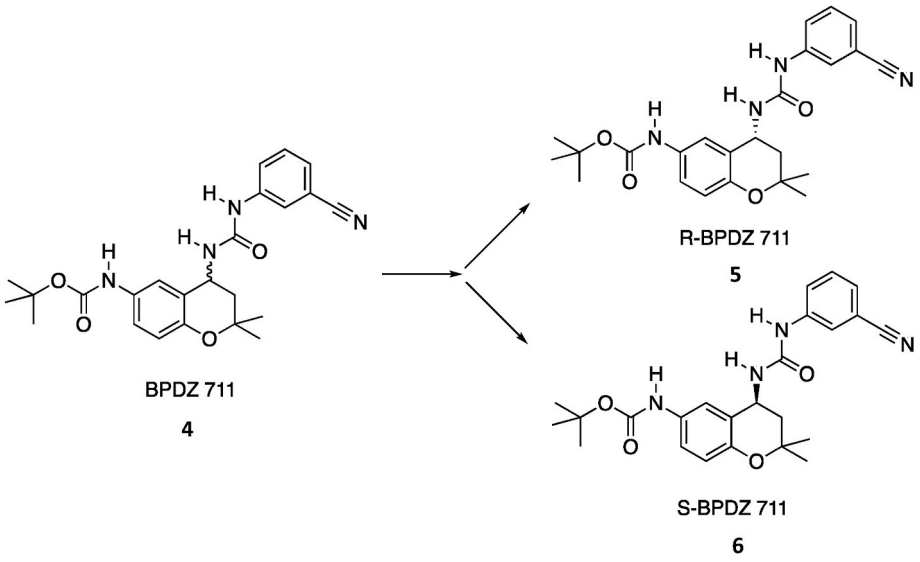


**Fig. 2.** The structure of the racemate BPDZ 711 (**4**) and its two enantiomers, R-BPDZ 711 (**5**) (or BPDZ 811) and S-BPDZ 711 (**6**) (or BPDZ 812).

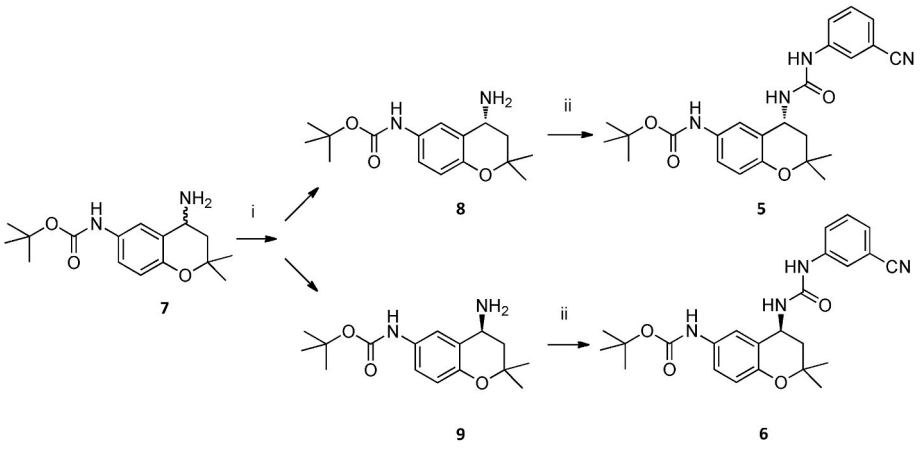


**Scheme 1.** Reagents: i: Chiralcel OD-H; ii: 3-CN-$C_6H_4NCO$.

forms (Fig. 6; A′ and A″) in DMSO. The NH(**3**) proton of the two compounds is easily identified because it appears as a doublet due to a coupling with the C-H proton at the 4-position of the heterocycle.

The $^1$H two-dimensional NOE spectroscopy (NOESY) experiment performed on both compounds by saturation of the signal of the N-H proton directly attached to the phenyl ring [Fig. 8D: NH(**2**) for BPDZ 711 (**4**); Fig. 8E: NH(**1**) for **12**] indicated that, ostensibly, the NH(**3**) proton of BPDZ 711 (**4**) was not in close proximity to the NH(**2**) proton; this suggests that the urea compound in solution may adopt another conformation where the two protons at a distance from each other (*i.e.*, conformations B, C or D, Fig. 6; conf. C, Fig. 8A). In contrast, the same experiment performed on the thiourea compound **12** clearly indicated that the two NH protons of the thiourea group are near to each other, supporting the view that conformation A dominates for this compound.

Consequently, the investigations into the conformational behavior of BPDZ 711 (**4**) reveal that this drug, existing in multiple conformations in solution, may not necessarily adopt the same 3D conformation (*i.e.*, the low energy conformation A, Fig. 6) when interacting with its various biological targets. Supporting this observation, molecular docking studies previously performed on human SIRT1 and SIRT2 confirmed that the R-enantiomer of BPDZ 711 (**4**), identified as the preferred enantiomer interacting with SIRT1 and SIRT2, adopts conformation C (Fig. 6) during interaction with the binding sites on the two enzymes [7].

### 2.2. Biological assays

#### 2.2.1. Inhibition of insulin release from rat pancreatic islets

In previous studies, the racemic compound BPDZ 711 (**4**) induced a concentration-dependent inhibition of glucose-induced insulin release from isolated and incubated rat pancreatic islets (Table 1) [5]. The present data further revealed that, under identical experimental conditions, BPDZ 811 (**5**), the R-enantiomer of BPDZ 711, also caused a marked dose-dependent inhibition of the glucose-stimulated insulin secretory process. The $IC_{50}$ value for the inhibitory effect of BPDZ 811 (**5**) on insulin release was 270 nM, close to that of BPDZ 711 (**4**) (Table 1). In contrast, BPDZ 812 (**6**), the S-enantiomer of BPDZ 711 (**4**), failed to affect insulin secretion in the nanomolar range of concentrations and exhibited an $IC_{50}$ value above 10 μM (Table 1).

#### 2.2.2. Oxygraphy measurements on K-562 cells

The effects of the two enantiomers of BPDZ 711 (**4**) on the $O_2$ consumption rate (OCR) were measured by oxygraphy in K-562 cells. Fig. 9A–B report representative slope curves obtained from K-562 cells treated with compounds **4** (BPDZ 711), **5** (BPDZ 811), and **6** (BPDZ 812) at a final concentration of 10 μM. Compared to controls (experiments carried out without the drug or with DMSO, which is the solvent used to prepare stock solutions of the studied compounds) (Fig. 9A, upper slope

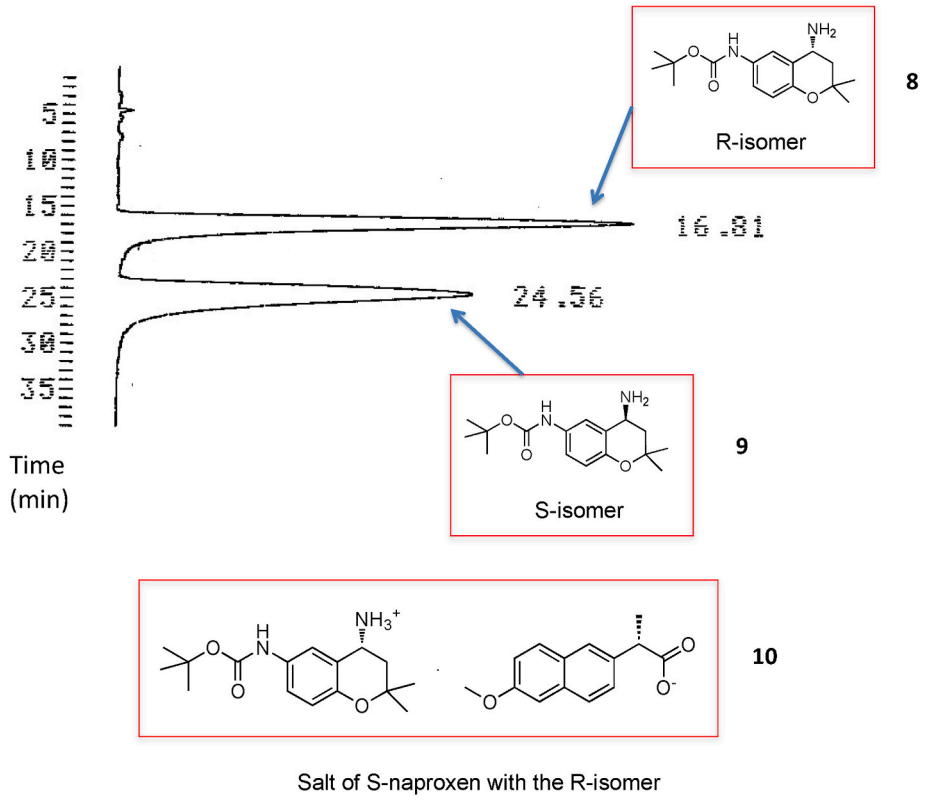


**Fig. 3.** Preparative chromatographic purification was performed on the Chiralcel OD-H column with the 4-amino-substituted racemate **7**, providing the separation of the two enantiomers **8** (retention time (rt): 16.81 min) and **9** (rt: 24.56 min). Compound **10** is the S-naproxen salt of **8**.

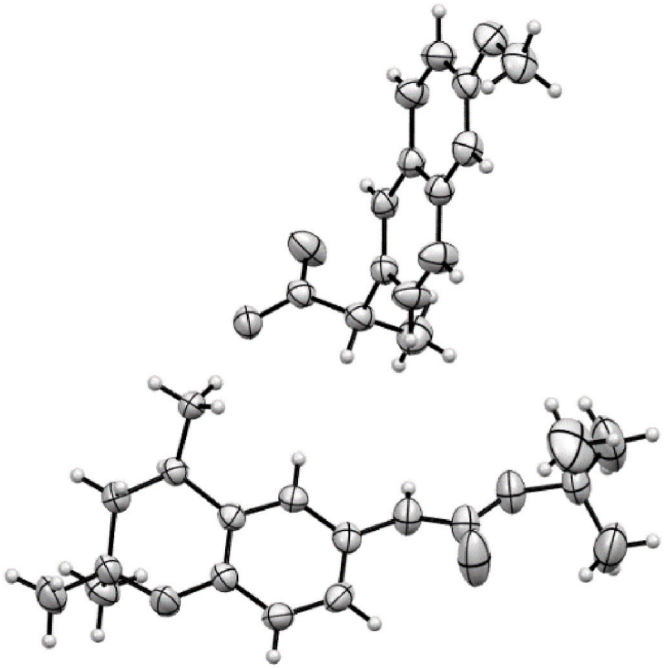

**Fig. 4.** Crystal structure of **10** identified as the S-naproxen salt of the R-isomer **8**.

curve), compound **4** (BPDZ 711) strongly decreased the routine respiratory rate (Fig. 9A, lower slope curve). The two enantiomers of BPDZ 711 (**4**) exhibited distinct profiles (Fig. 9B). The R-enantiomer BPDZ 811 (**5**) exhibited a similar impact on the OCR as the racemate BPDZ 711 (**4**) (Fig. 9B, upper slope curve), while the S-enantiomer BPDZ 812 (6) showed no significant effect (Fig. 9B, lower slope curve).

Fig. 10 summarizes the comparative effects of the three compounds (10 μM) on the cellular respiratory parameters: basal respiration [Routine (control without product) + Product)], leak respiration (Leak: residual respiration after inhibition of ATP synthase by oligomycin) and maximal respiratory capacity (ETSmax: electron transfer system percentage) in the presence of carbonyl cyanide 4-(trifluoromethoxy)phenylhydrazone (FCCP). To understand the intrinsic effect of the compounds on the cellular respiration rate of K-562 cells, a set of experiments was performed by first monitoring the slope of the curve (cells without adding a compound) and comparing it to the effect observed in the presence of the different compounds. Mitochondrial parameters, such as proton and electron leaks, were analyzed using specific inhibitors, such as oligomycin, to monitor whether or not oxidative phosphorylation was coupled with respiration at the level of complex V (ATP synthase). This step was followed by increasing amounts of FCCP to evaluate the maximal respiratory capacity, as previously reported [17].

Fig. 10 shows that, when the compounds were added at 10 μM after the onset of cellular respiration, the basal respiration (routine: before the addition of compound) was significantly altered by BPDZ 711 (**4**) and BPDZ 811 (**5**) (OCR decreased: see "product" in Fig. 10). In contrast, BPDZ 812 (**6**) had little effect. After the oligomycin-induced leak, BPDZ 711 (**4**) and BPDZ 811 (**5**), in similar conditions, continued to reduce mitochondrial enzyme complex activity, while BPDZ 812 (**6**) was ineffective. Both compounds affected the maximal respiratory capacity of K-562 cells, whereas BPDZ 812 (**6**) exhibited minimal activity.

### 2.2.3. *Inhibition of histone deacetylase class III enzymes*

The inhibitory potential of the racemate **4** (BPDZ 711), its R-enantiomer **5** (BPDZ 811), and its S-enantiomer **6** (BPDZ 812) was tested against selected HDAC class III activities including SIRT1, SIRT2 and

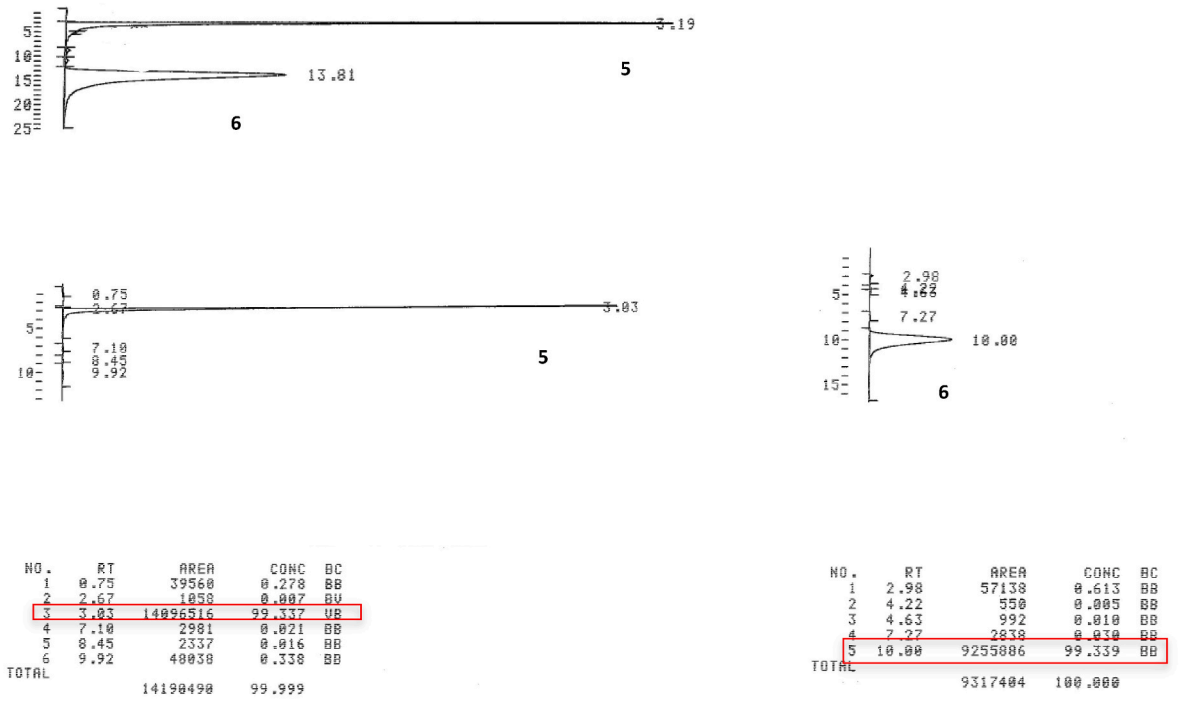


**Fig. 5.** Preparative chromatographic purification of the racemate BPDZ 711 (**4**) on the Chiralcel OD-H column leading to the separation of the two isomers R-BPDZ 711 (**5**) and S-BPDZ 711 (**6**).

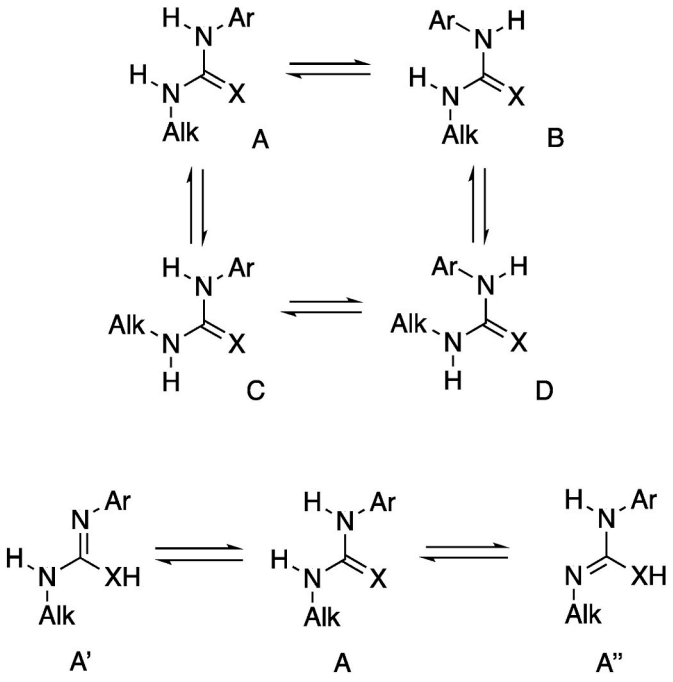


**Fig. 6.** The ureas (X = O) and the thioureas (X = S) bearing alkyl/aryl substituents on the nitrogen atoms are expected to adopt four preferential low energy conformations (A, B, C, and D), as well as multiple tautomeric forms (for conformation A; tautomeric forms A′ and A″).

SIRT3 (Table 2). The corresponding $IC_{50}$ values revealed that the R-enantiomer **5** was the active eutomer exhibiting lower $IC_{50}$ values against SIRT1 and SIRT2 compared to the racemate BPDZ 711 (**4**), while the S-enantiomer **6** showed no activity. All compounds were inactive against SIRT3.

To extend our *in vitro* results on SIRT1/2 enzyme inhibition, the two separated enantiomers of BPDZ 711 (**4**) were then tested *in cellulo*. Their potential to modulate the acetylation levels of histone and non-histone proteins was assessed in the human CML cell line K-562. Cells were treated for 24 h with BPDZ 811 (**5**) and BPDZ 812 (**6**) at concentrations of 0.1–25 μM (Fig. 11). The pan-HDAC inhibitor suberoylanilide hydroxamic acid (SAHA) served as a positive control to induce protein acetylation. We observed a concentration-dependent increase in α-tubulin and histone H4 acetylation levels after treatment with BPDZ 811 (**5**), consistent with previously reported results for BPDZ 711 (**4**) [9], but not with BPDZ 812 (**6**). The R-enantiomer **5** initiated protein acetylation at low concentrations (0.5 μM). These findings confirmed that the R-enantiomer **5** is the eutomer inhibiting the sirtuin-mediated deacetylation of histone and non-histone proteins in K-562 leukemia cells.

The R-enantiomer of BPDZ 711 (**5**) functions as the eutomer by directly inhibiting the deacetylase activity of sirtuin enzymes SIRT1 and SIRT2 in K-562 leukemia cells. This inhibition likely occurs through the binding of compound **5** to the catalytic domain of these enzymes, where its specific three-dimensional configuration allows for optimal interactions such as hydrogen bonds or hydrophobic contacts within the active site, thus interfering with the ability of SIRTs to deacetylate substrate proteins. Additionally, compound **5** may compete with the binding of $NAD^+$, the essential cofactor of sirtuin-catalyzed deacetylation reactions, disrupting sirtuin activity. As a result, there is an increase in the acetylation levels of SIRT1 and SIRT2 substrates, including histone H4 and non-histone proteins like α-tubulin, respectively. Elevated histone acetylation leads to a more relaxed chromatin structure, promoting transcriptional activation of genes involved in cell cycle arrest or apoptosis. Increased acetylation of α-tubulin affects microtubule stability and dynamics, potentially disrupting mitotic spindle formation and inhibiting cell division. Altogether. these findings confirm that BPDZ 811 (**5**) is a potent and specific inhibitor of sirtuin-mediated deacetylation, underscoring the importance of molecular configuration in drug design and efficacy.

### 2.2.4. *Effect on extracellular pH of K-562 treated cells*

After treating K-562 cells with increasing concentrations of the two

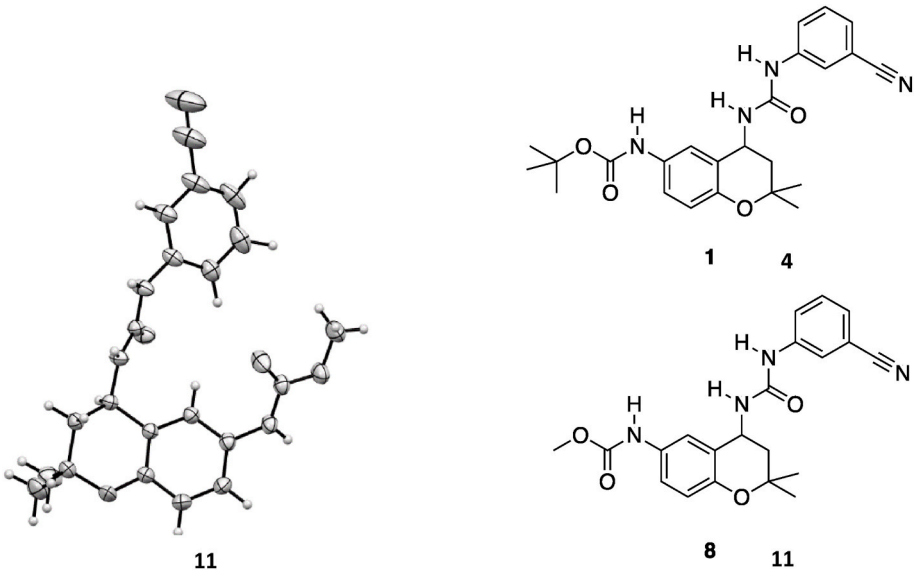


**Fig. 7.** Crystal structure of compound **11** (illustrated as the R-isomer), the "methyl" analog of the "tert-butyl" compound **4**.

enantiomers (0.1–50 μM), the extracellular pH significantly decreased after 24, 48, and 72h of treatment with the R-enantiomer BPDZ 811 (**5**), similar to previously reported results for BPDZ 711 [9], but not with the S-enantiomer BPDZ 812 (**6**) (Fig. 12). The acidification of the extracellular medium increased with treatment duration, reaching its peak at concentrations of BPDZ 811 between 1 and 5 μM. This acidification by BPDZ 811 (**5**) could be attributed to an enhanced lactic acid release due to an increased glycolytic rate, as previously shown with the racemate **4** (BPDZ 711) [9].

### 2.2.5. *Effect of BPDZ 711 enantiomers on the proliferation and viability of cancer and healthy cells*

The effect of the two enantiomers BPDZ 811 (**5**) and BPDZ 812 (**6**) was tested after 24, 48, and 72 h of treatment on K-562 cell proliferation and viability (Fig. 13A and Table 3). The R-enantiomer BPDZ 811 (**5**) was found to be more potent than the S-enantiomer BPDZ 812 (**6**) in inhibiting CML cell growth. The growth inhibition $GI_{50}$ values after 72 h of treatment were found to be 0.9 μM for BPDZ 811 (**5**) and 14.7 μM for BPDZ 812 (**6**) to be compared to the 1.3 μM reported for the racemate BPDZ 711 (**4**) [9]. Furthermore, compound **5** did not exhibit significant acute toxicity [lethal dose $LD_{50}$ value > 50 μM] on K-562 cells, suggesting that this enantiomer primarily acts as a cytostatic compound against cancer cells similar to the racemate BPDZ 711 (**4**) [9] (Fig. 13A).

After 3 days of treatment, compounds BPDZ 811 (**5**) and BPDZ 812 (**6**) did not exhibit significant acute toxicity on the viability of non-proliferating peripheral blood mononuclear cells (PBMCs) from healthy adult donors (Fig. 13B). Phytohemagglutinin (PHA) was used to stimulate PBMCs into the cell cycle and cause their immune activation, a common immune proliferation model [18]. The effect of the two enantiomers BPDZ 811 (**5**) and BPDZ 812 (**6**) was assessed on the proliferation and viability of proliferating PBMCs (P_PBMCs) (Fig. 13C). The results showed that none of the compounds exhibited significant acute toxicity on PHA-stimulated PBMCs, with $LD_{50}$ values > 50 μM (Table 4). However, the R-enantiomer **5** was found to be a more potent inhibitor of P_PBMC proliferation ($GI_{50}$ = 7.2 μM) than the S-enantiomer **6** ($GI_{50}$ > 50 μM) or the racemate **4** ($GI_{50}$ = 16.6 μM as previously reported in Ref. [9]) (Table 4). The R-enantiomer **5** displayed a favorable differential toxicity for cancer cells with a selectivity factor of 8, comparable to that reported for the racemate **4** [9] (Table 4).

### 2.2.6. *Effect of BPDZ 711 enantiomers on cell death*

We recently reported that compound BPDZ 711 (**4**) induced non-canonical cell death in K-562 cells in a time- and concentration-dependent manner. After 5 days of treatment, a necrotic cell death was observed at 5–10 μM, while an apoptotic cell death occurred at higher concentrations (25–50 μM) [9]. In the case of the separated enantiomers of BPDZ 711 (**4**), only the R-enantiomer **5** reproduced the effects of **4** (Fig. 14A). After 5 days of treatment, a majority of propidium iodide-positive (*i.e.,* necrotic) cells were observed with 5 at 2.5–10 μM, whereas the S-enantiomer **6** triggered primarily apoptotic cell death but only at high concentrations (25–50 μM).

When comparing the effect of the enantiomers of BPDZ 711 (**4**) on cell death in P_PBMCs, we showed that the treatments mainly triggered apoptosis but only at the highest tested concentrations (Fig. 14B). Additionally, $LD_{50}$ values (Table 5) revealed that 5 days of incubation with the R-enantiomer **5** selectively killed CML cells compared to healthy proliferating cells with a selectivity factor of 20, consistent with the published results for the racemate **4** [9]. In contrast, the S-enantiomer **6** showed no selectivity.

The release of high mobility group box (HMGB1) in the extracellular medium may reflect cellular stress associated with histone acetylation [19]. Necrotic and damaged cells, but not apoptotic cells, passively release HMGB1 [19]. As shown in Fig. 14C, only the R-enantiomer of BPDZ 711 (**4**) induced HMGB1 release from K-562 cells, even at low concentrations (0.25 μM). At higher concentrations (10 and 25 μM), a progressive decrease in HMGB1 release was observed, as expected from apoptotic cells.

Elevated concentrations of BPDZ 711 (**4**) or 811 (**5**) treatment lead to more rapid canonical cell death induction (*i.e.* apoptotic) compared to non-toxic but epigenetically-active concentrations associated with non-canonical cell death (*i.e.* controlled necrosis) (Fig. 14) [9]. This rapid induction of apoptosis is associated with RNA damage and ER stress (data not shown). Accordingly, other studies have reported that higher concentrations of HDAC inhibitors induce DNA damage [20] and/or ER stress [21] that are not observed at lower concentrations. These observations are likely due to potential off-target effects achieved at higher concentrations by any chemotherapeutic drug generating oxidative stress and/or genotoxicity. Moreover, decreased expression or activity of histone acetyltransferases (HATs) by (post)transcriptional or (post) translational mechanisms was described [22]. Similarly, increased expression/activity of SIRTs or other HDACS by (post)transcriptional or (post) translational mechanisms were previously hypothesized [23]. Such regulatory mechanisms could also explain the differential effect observed at the highest concentrations. Finally, modulation of the

availability of metabolic cofactors of HDACs/HATS could impact the activity of these enzymes [24].

## 3. Conclusion

The synthesis of the two enantiomers of BPDZ 711 (**4**) was achieved through the reaction of 3-cyanophenyl isocyanate with the R- and S-amine precursors, which were obtained by chiral column chromatography. Moreover, the two enantiomers were separated from the racemate by preparative chiral column chromatography, yielding the R- and the S-isomers with high enantiomeric purity [enantiomeric excess: 99.0 % for R-BPDZ 711 (**5**) and 98.7 % for S-BPDZ 711 **6**)].

A conformational study revealed that BPDZ 711 (**4**) and its separated enantiomers may exist in multiple conformations in solution and may not necessarily adopt the same conformation when interacting with their diverse biological targets.

The R- and S-enantiomers of BPDZ 711 (**4**) were evaluated in different biological assays (inhibition of insulin release from pancreatic β-cells, oxygraphic measurements in K-562 cells, inhibitory activity on SIRT1/2, increased protein acetylation in K-562 cells, acidification of the extracellular pH from K-562 treated cells, inhibition of K-562 cell proliferation and viability, differential effect on viability and proliferation of healthy PBMCs, alteration of the nuclear morphology of K-562 cells and HMGB1 release). In all assays, the R-enantiomer of BPDZ 711 (BPDZ 811, **5**) was consistently more active than the S-enantiomer (BPDZ 812, **6**), supporting the conclusion that the R-enantiomer **5** is the reference compound for future anticancer drug discovery development.

## 4. Experimental section

### 4.1. Chemistry

#### 4.1.1. Synthesis and enantiomeric separation

*4.1.1.1. General procedures.* Melting points were determined on a Büchi Tottoli capillary device and were uncorrected. The $^{1}H$ and $^{13}C$ NMR spectra were recorded on a Bruker Advance (500 MHz) instrument using deuterated dimethyl sulfoxide ($d_6$-DMSO) as the solvent with tetramethylsilane (TMS) as an internal standard; chemical shifts are reported in $\delta$ values (ppm) relative to that of internal TMS. The abbreviations s = singlet, d = doublet, q = quadruplet, m = multiplet, dd = doublet of doublet, and bs = broad singlet are used throughout. Elemental analyses

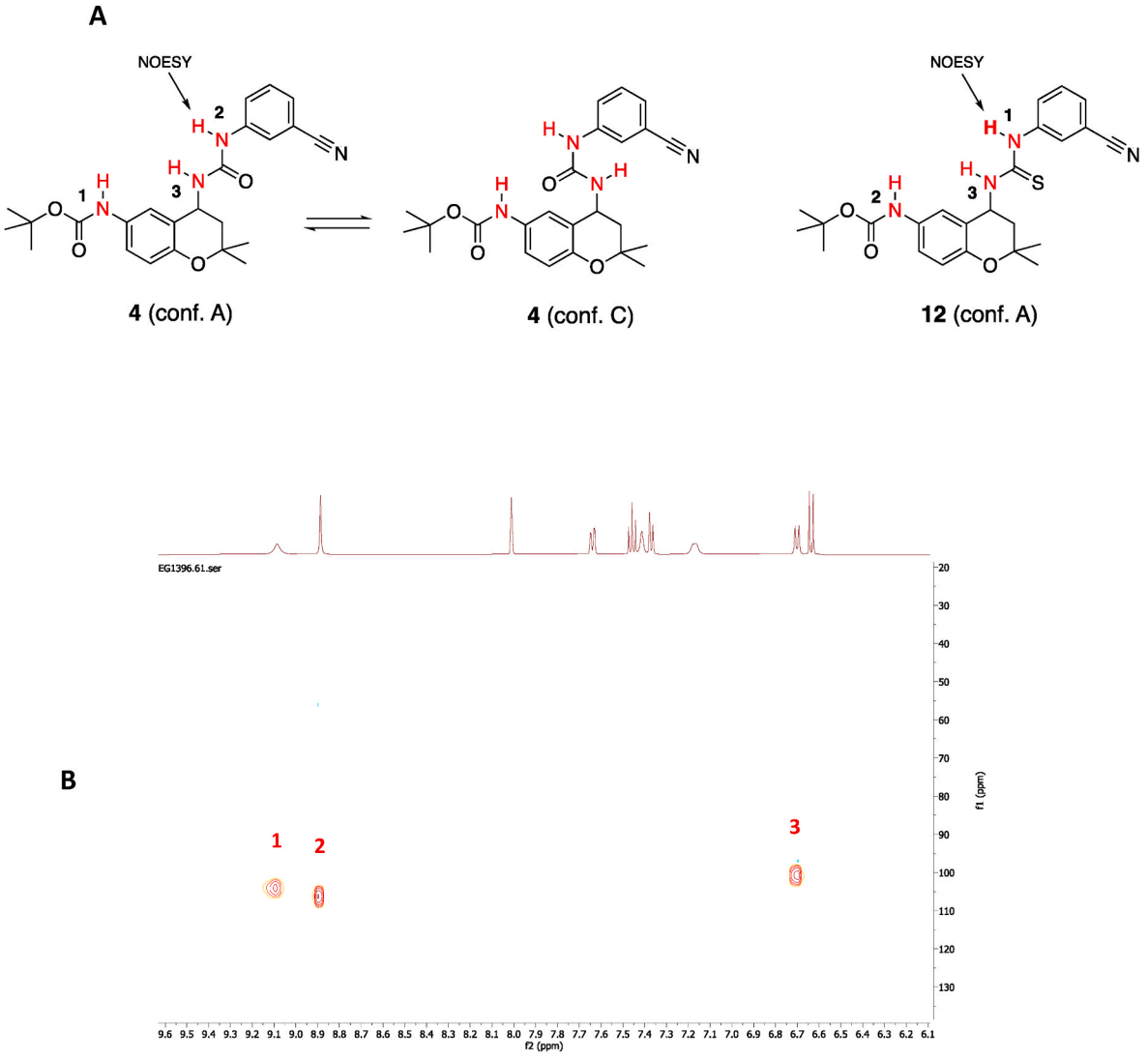


**Fig. 8. A:** Structure of compound **4** (showing a possible equilibrium between conformation A and conformation C) and its thiourea analog compound **12**. **B-C:** $^{15}N$-$^{1}H$ HSQC spectrum of compound **4** (**B**) and compound **12** (**C**) confirming that the hydrogen atoms are linked to the nitrogen atoms of the urea [NH(**2**) and NH(**3**)] and the thiourea [NH(**1**) and NH(**3**)] functions. **D-E:** $^{1}H$ two-dimensional NOE spectroscopy (NOESY) experiment performed on **4** (**D**) and **12** (**E**) by saturation of the signal of the N-H proton directly linked to the phenyl ring.

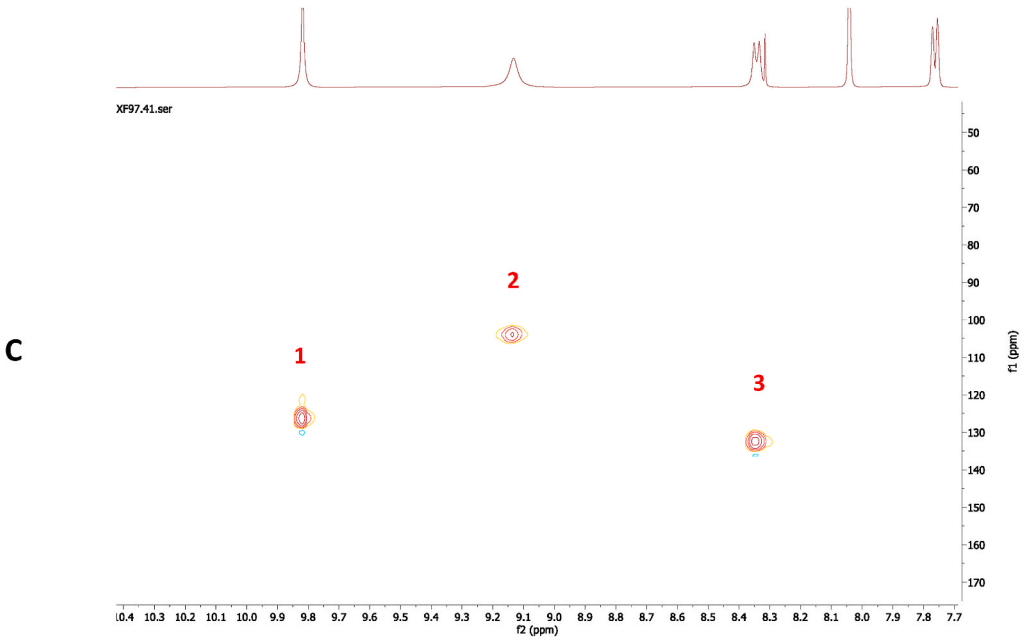


**Fig. 8.** (*continued*).

**Table 1**
Effect of BPDZ 711 (4) and its enantiomers BPDZ 811 (5, R-BPDZ 711) and BPDZ 812 (6, S-BPDZ 711) on the glucose-induced insulin release from rat pancreatic islets.

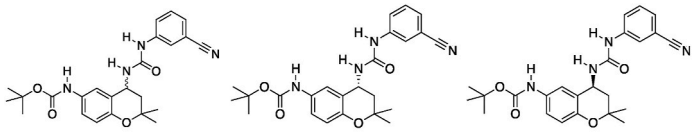

BPDZ 711 (4) BPDZ 811 (5) BPDZ 812 (6)

| Compound | Residual insulin secretion[a] | | | | $IC_{50}$ (μM) |
|---|---|---|---|---|---|
| | % at 10 μM | % at 1 μM | % at 0.5 μM | % at 0.1 μM | |
| BPDZ 711 (**4**) | 7.4 ± 1.0 (25)[b] | 15.6 ± 1.2 (20)[b] | 28.6 ± 1.8 (21)[b] | 82.0 ± 4.6 (30)[b] | 0.24[b] |
| BPDZ 811 (**5**) | 9.3 ± 0.9 (21) | 22.8 ± 3.3 (15) | 31.0 ± 3.1 (15) | 89.7 ± 4.5 (16) | 0.27 |
| BPDZ 812 (**6**) | 58.6 ± 2.6 (23) | 103.1 ± 7.0 (15) | 107.9 ± 5.7 (15) | 109.5 ± 9.5 (15) | >10 |

[a] Percentage of residual insulin release from rat pancreatic islets incubated in the presence of 16.7 mM glucose [mean ± SEM (n)].
[b] Published compound and results (ref. [5]).

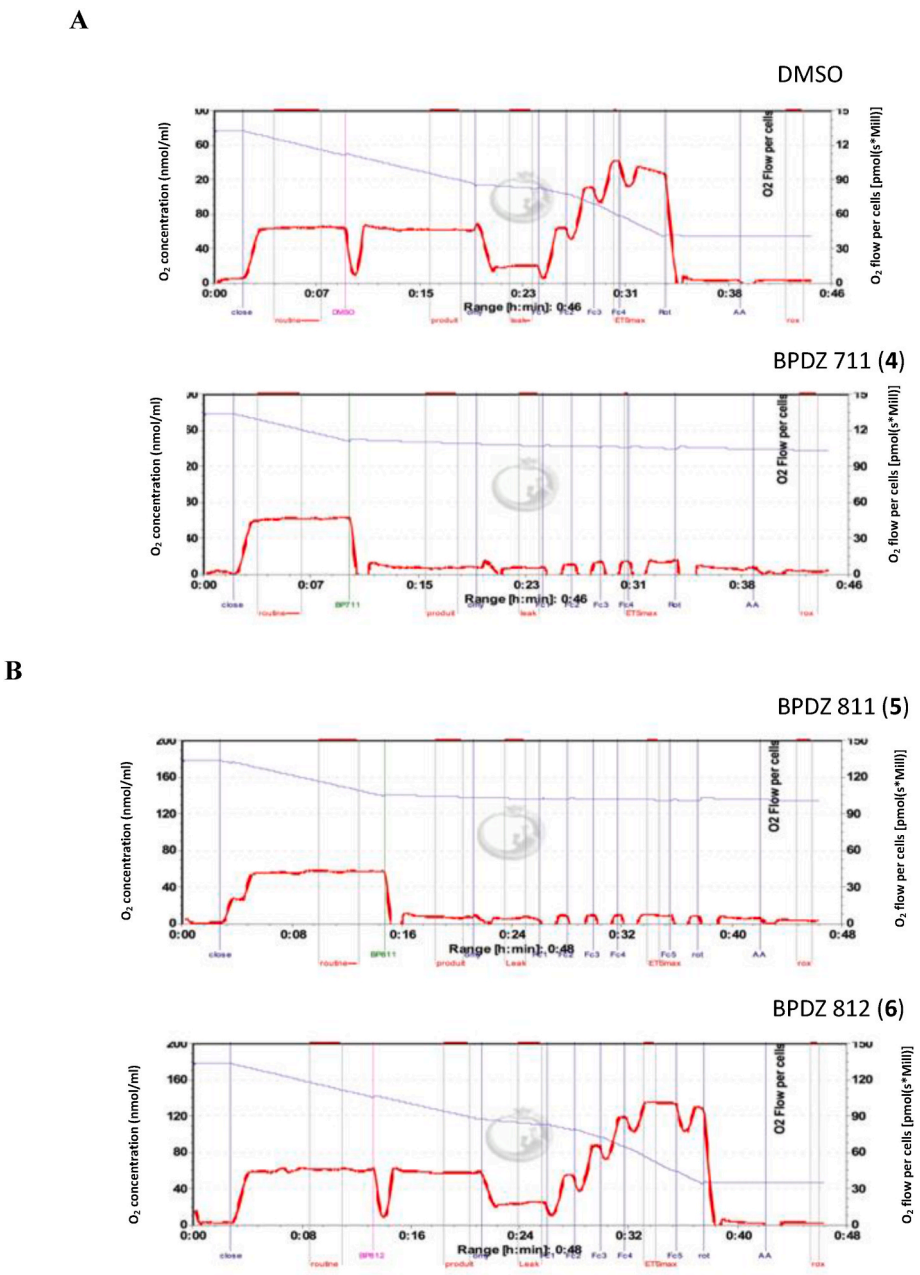


**Fig. 9.** Representative slope curves obtained from K-562 cells using oxygraphy in the presence of **4** (BPDZ 711), **5** (BPDZ 811), and **6** (BPDZ 812) at a final concentration of 10 μM: (**A**) control experiment (upper panel: DMSO) compared to the experiment conducted with **4** (lower panel: BPDZ 711); (**B**) experiments conducted with **5** (upper panel: BPDZ 811) and **6** (lower panel: BPDZ 812).

(C, H, N, S) were realized on a Thermo Scientific Flash EA 1112 elemental analyzer and were within ±0.4 % of the theoretical values for carbon, hydrogen, and nitrogen. This analytical method certified a purity of ≥95 % for each tested compound. All reactions were routinely checked by TLC on silica gel Merck 60 F254. Compounds BPDZ 711 (**4**), **11**, and **12** were obtained as previously described [4,5].

*4.1.1.2. Enantiomeric separation of the amines **8** and **9**.* The following chromatographic conditions were used for the separation of the two enantiomers of compound **7** (Scheme 1). Precolumn: Chiralcel OD-H 10 × 20 mm, 5 μm; column: Chiralcel OD-H 2 × 25 cm, 5 μm; mobile phase: hexane/isopropanol (60:40); sample of compound injected: 25 mg/mL; injection volume: 1 mL; flow rate: 10 mL/min.

A sample of compound **8** was converted into the S-naproxenate salt after a reaction of the amine with an equimolar amount of S-naproxen in methanol (compound **10**: 50 mg; 0.17 mmol + S-naproxen: 39.4 mg; 0.15 mmol). The solution was subjected to a slow evaporation until salt crystals appeared. The crystals were carefully collected and dried.

**(*R*)-6-[(*tert*-butoxycarbonyl)amino]-2,2-dimethylchroman-4-aminium (*S*)-2-(6-methoxynaphthalen-2-yl)propanoate (10).** White crystals; $^1$H NMR (DMSO-$d_6$) $\delta$ 1.17 (s, 3H, C$H_3$), 1.32 (s, 3H, C$H_3$), 1.43 (d, J = 7.1 Hz, 3H, C$H_{3\ nap}$), 1.45 (s, 9H, NHCOOC(C$H_3$)$_3$), 1.52 (m, 1H, 3-*Ha*), 2.00 (dd, J = 13.1 Hz/6.0 Hz, 3-*Hb*), 3.39 (bs, 3H, N$H_3^+$), 3.77 (q, J = 7.1 Hz, 1H, C$H_{nap}$), 3.82 (dd, J = 11.0 Hz/6.0 Hz, 1H, 4-*H*), 3.86 (s, 3H, OC$H_{3\ nap}$), 6.55 (d, J = 8.7 Hz, 1H, 8-*H*), 7.05 (d, J = 7.6 Hz, 1H, 7-*H*), 7.14 (dd, J = 8.9 Hz/2.1 Hz, 1H, 7-$H_{nap}$), 7.28 (d, J = 1.4 Hz, 1H, 5-$H_{nap}$), 7.40 (d, J = 8.3 Hz, 1H, 2-$H_{nap}$), 7.64 (s, 1H, 5-*H*), 7.70 (s, 1H, 10-$H_{nap}$), 7.75 (d, J = 8.6 Hz, 1H, 3-$H_{nap}$), 7.78 (d, J = 9.0 Hz, 1H, 8-$H_{nap}$), 8.97 (s, 1H, N*H*COOC(CH$_3$)$_3$). Anal. ($C_{30}H_{38}N_2O_6$) theoretical: C, 68.94; H, 7.33; N, 5.36. Found: C, 68.89; H, 7.25; N, 5.73.

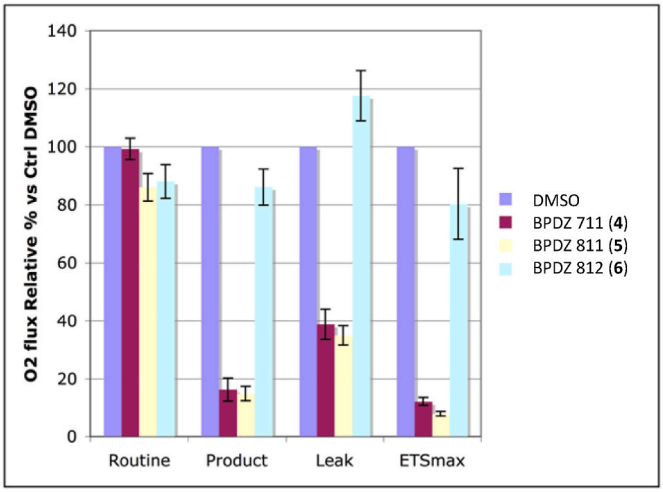


**Fig. 10.** Summary of the cellular respiratory parameters obtained with **4** (BPDZ 711), **5** (BPDZ 811) and **6** (BPDZ 812) at a concentration of 10 μM compared to the control (DMSO) on K-562 cells [mean ± SD (n = 3)]: basal respiration [Routine (control) + Product], leak respiration, and maximal capacity of the respiratory chain (ETSmax).

**Table 2**
Inhibitory activity of BPDZ 711 (4) and its enantiomers BPDZ 811 (5, R-BPDZ 711) and BPDZ 812 (6, S-BPDZ 711) on SIRT1, -2, and -3 activities.

| Compound | $IC_{50}$ (μM)[a] | | |
|---|---|---|---|
| | SiRT1 | SiRT2 | SiRT3 |
| BPDZ 711 (**4**) | 6.6 ± 1.0 | 4.4 ± 1.5 | >100 |
| BPDZ 811 (**5**) | 3.8 ± 1.3 | 3.2 ± 0.6 | >100 |
| BPDZ 812 (**6**) | >100 | >100 | >100 |

[a] $IC_{50}$ values: the concentration of drug required to inhibit 50 % of the specified sirtuin (SIRT) activity (mean ± SD of 3 independent experiments). $IC_{50}$ values were calculated from the inhibitory dose–response curves using the negative solvent control DMSO set to 100 % activity.

#### 4.1.2. *Synthesis of compounds **5** and **6***

Compounds BPDZ 811 (**5**) and BPDZ 812 (**6**) were obtained according to the synthetic process previously described for the racemic compound BPDZ 711 (**4**) [5], starting from compounds **8** and **9**, respectively.

#### 4.1.3. *Enantiomeric separation of the enantiomers of BPDZ 711 (**4**)*

The following chromatographic conditions were used for the separation of the two enantiomers of BPDZ 711 (**4**). Precolumn: Chiralcel OD-H 10 × 20 mm, 5 μm; column: Chiralcel OD-H 2 × 25 cm, 5 μm; mobile phase: hexane/isopropanol (50:50); sample of compound injected: 25 mg/mL; injection volume: 1 mL; flow rate: 10 mL/min. The elution order is R-BPDZ 711 (**5**) and S-BPDZ 711 (**6**) [enantiomeric excess: 99.0 % for R-BPDZ 711 (**5**) and 98.7 % for S-BPDZ 711 (**6**)]. After 6 runs of 25 mg/mL of the racemate (150 mg BPDZ 711), the following amount of each enantiomer was obtained; R-enantiomer: 63 mg (42 %); S-enantiomer: 70 mg (47 %).

**(*R*)-*N*-3-cyanophenyl-*N*'-(6-tert-butoxycarbonylamino-3,4-dihydro-2,2-dimethyl-2H-1-benzopyran-4-yl)urea** (**5**). White solid; melting point: 188.5–191 °C. $^1$H NMR (DMSO-$d_6$) $\delta$ 1.25 (s, 3H, C*H*$_3$), 1.36 (s, 3H, C*H*$_3$), 1.42 (s, 9H, NHCOOC(C*H*$_3$)$_3$), 1.73 (m, 1H, 3-*Ha*), 2.08 (dd, J = 13.2 Hz/6.3 Hz, 3-*Hb*), 4.93 (dd, J = 9.0 Hz/8.1 Hz, 1H, 4-*H*), 6.63 (d, J = 8.8 Hz, 1H, 8-*H*), 6,73 (d, J = 8.6 Hz, 1H, CHN*H*CONHAr), 7.17 (d, J = 6.7 Hz, 1H, 7-*H*), 7.37 (d, J = 7.6 Hz, 1H, 4′-*H*), 7.41 (bs, 1H, 5-*H*), 7.46 (t, J = 8.0 Hz, 1H, 5′-*H*), 7.64 (d, J = 9.4 Hz, 1H, 6′-*H*), 8.01 (d, J = 1.6 Hz, 1H, 2′-*H*), 8.92 (s, 1H, CHNHCON*H*Ar), 9.07 (bs, 1H, N*H*COOC(CH$_3$)$_3$). Anal. ($C_{24}H_{28}N_4O_4$) theoretical: C, 66.04; H, 6.47; N, 12.84. Found: C, 65.92; H, 6.72; N, 13.03.

**(*S*)-*N*-3-cyanophenyl-*N*'-(6-tert-butoxycarbonylamino-3,4-dihydro-2,2-dimethyl-2H-1-benzopyran-4-yl)urea** (**6**). White solid; melting point: 178–182 °C. $^1$H NMR (DMSO-$d_6$) $\delta$ 1.25 (s, 3H, C*H*$_3$), 1.36 (s, 3H, C*H*$_3$), 1.42 (s, 9H, NHCOOC(C*H*$_3$)$_3$), 1.73 (m, 1H, 3-*Ha*), 2.08 (dd, J = 13.2 Hz/6.2 Hz, 3-*Hb*), 4.93 (dd, J = 9.0 Hz/8.1 Hz, 1H, 4-*H*), 6.63 (d, J = 8.8 Hz, 1H, 8-*H*), 6,73 (d, J = 8.5 Hz, 1H, CHN*H*CONHAr), 7.17 (d, J = 7.1 Hz, 1H, 7-*H*), 7.37 (d, J = 7.6 Hz, 1H, 4′-*H*), 7.41 (bs, 1H, 5-*H*), 7.46 (t, J = 8.0 Hz, 1H, 5′-*H*), 7.64 (d, J = 8.4 Hz, 1H, 6′-*H*), 8.01 (t, J = 1.5 Hz, 1H, 2′-*H*), 8.92 (s, 1H, CHNHCON*H*Ar), 9.07 (s, 1H, N*H*COOC(CH$_3$)$_3$). Anal. ($C_{24}H_{28}N_4O_4$) theoretical: C, 66.04; H, 6.47; N, 12.84. Found: C, 65.85; H, 6.51; N, 12.56.

#### 4.1.4. *Crystallographic measurements on compound **10** and compound **11***

Single-crystal X-ray diffraction data were collected using the Oxford Diffraction Gemini R Ultra diffractometer (Cu Kα, multilayer mirror, Ruby CCD area detector). Data collection, unit cell determination, and data reduction were carried out using the CrysAlisPRO software package [25]. Using Olex2 [26] and ShelXle [27], the structure was solved with the SHELXT 2015 [28] structure solution program by Intrinsic Phasing methods and refined by full-matrix least-squares on $|F|^2$ using SHELXL-2018/3 [26–29,29–31]. Non-hydrogen atoms were refined anisotropically. Hydrogen atoms were placed on calculated positions in

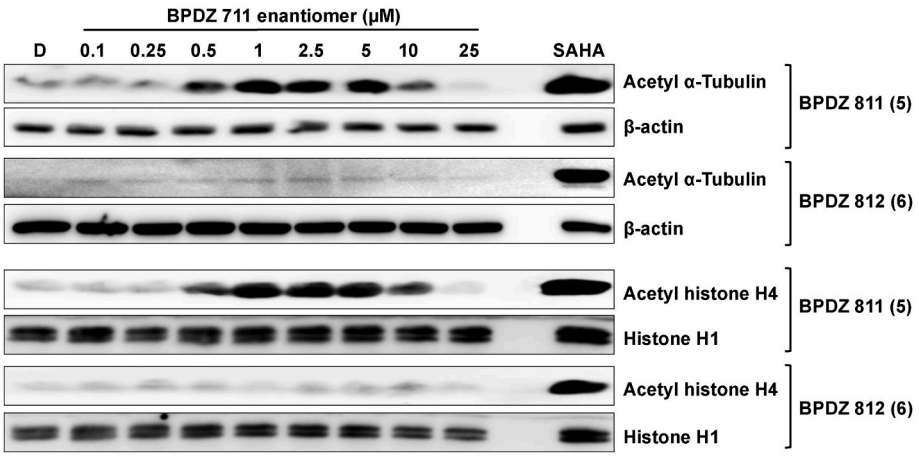


**Fig. 11.** Effects of BPDZ 711 enantiomers on protein acetylation in K-562 cells. Cells were treated with either DMSO (D) as a vehicle or the indicated concentrations of BPDZ 711 enantiomers: BPDZ 811 (R-BPDZ 711) and BPDZ 812 (S-BPDZ 711). After 24h of incubation, cells were analyzed for the levels of α-tubulin and histone H4 acetylation by Western blot. β-actin and histone H1 were used as loading controls for α-tubulin and histone H4, respectively. SAHA: (suberoylanilide hydroxamic acid, 2 μM) was used as a reference non-sirtuin pan-HDAC inhibitor. The immunoblot pictures are representative of three independent experiments.

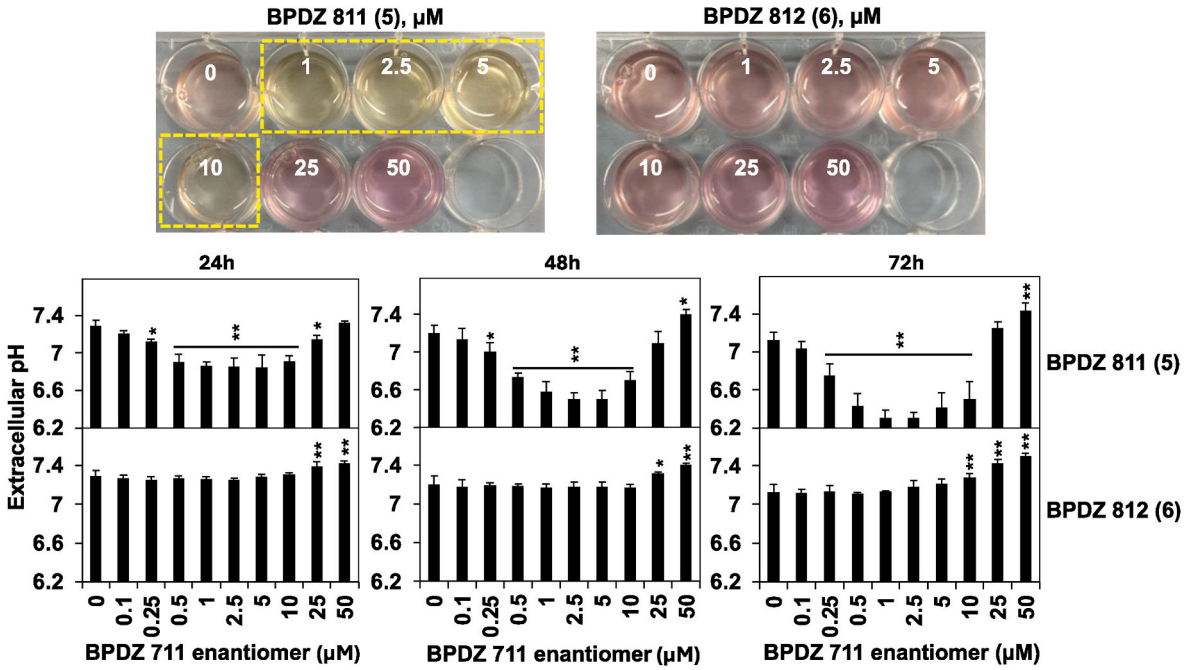


**Fig. 12.** Effect of BPDZ 711 enantiomers on extracellular pH. K-562 cells were treated with increasing concentrations of BPDZ 711 enantiomers: BPDZ 811 (R-BPDZ 711) and BPDZ 812 (S-BPDZ 711) for up to 72h. Upper panel: after 48h of incubation, cell culture wells were photographed to document cell culture media color changes. Rectangles with dashed yellow lines indicate the range of concentrations of BPDZ 811, leading to enhanced medium acidification compared to the control. Images are representative of at least three independent experiments. Lower panel: extracellular pH measurements at the indicated time points. Data represent the mean ± SD of three independent experiments. P values were calculated by one-way ANOVA with Dunnett's multiple comparison test. * and ** indicate $P < 0.05$ and $P < 0.01$, respectively, versus control cells.

riding mode with temperature factors fixed at 1.2 times $U_{eq}$ of the parent carbon atoms (1.5 times for methyl groups).

Crystal Data for **10**: $C_{30}H_{38}N_2O_6$ ($M$ = 522.62 g/mol): monoclinic, space group $P2_1$ (no. 4), $a$ = 13.1090(8) Å, $b$ = 5.9511(4) Å, $c$ = 18.0407 (10) Å, $\beta$ = 93.239(6)°, $V$ = 1405.16(15) Å$^3$, $Z$ = 2, $T$ = 295(2) K, μ(Mo Kα) = 0.086 mm$^{-1}$, $D_{calc}$ = 1.235 g/cm$^3$, 20845 reflections measured (6.226° ≤ 2θ ≤ 52.842°), 5744 unique ($R_{int}$ = 0.0315, $R_{sigma}$ = 0.0290) which were used in all calculations. The final $R_1$ was 0.0359 (I > 2σ(I)), and w$R_2$ was 0.0863 (all data).

Crystal Data for **11**: $C_{21}H_{22}N_4O_4$ ($M$ = 394.42 g/mol): monoclinic, space group $I2/a$ (no. 15), $a$ = 16.2893(5) Å, $b$ = 9.2649(3) Å, $c$ = 25.9062(8) Å, $\beta$ = 97.897(3)°, $V$ = 3872.7(2) Å$^3$, $Z$ = 8, $T$ = 295(2) K, μ(Mo Kα) = 0.096 mm$^{-1}$, $D_{calc}$ = 1.353 g/cm$^3$, 19606 reflections measured (4.674° ≤ 2θ ≤ 65.564°), 6537 unique ($R_{int}$ = 0.0224, $R_{sigma}$ = 0.0277) which were used in all calculations. The final $R_1$ was 0.0497 (I > 2σ(I)), and w$R_2$ was 0.1399 (all data).

## 4.2. Biological assays

### 4.2.1. Insulin release from rat pancreatic islets

The method used to measure insulin release from incubated rat pancreatic islets was previously described [7].

### 4.2.2. Cell culture

The human chronic myelogenous leukemia K-562 cell line (Cat# ACC-10, Research Resource Identifier: CVCL_0004) was obtained from the Deutsche Sammlung für Mikroorganismen und Zellkulturen (Braunschweig, Germany). PBMCs from healthy adult human donors were isolated, as previously reported [32]. P_PBMCs were obtained and generated as previously described [32].

PBMCs and P_PBMCs were used with the approval of the National Research Ethics Committee of Luxembourg. PBMCs were isolated from blood obtained from the Red Cross (Luxembourg, Luxembourg) under the authorization LBMCC-2019-0002: "Assessment of toxicity of new drugs or drug combinations in preclinical development in non-proliferating peripheral blood mononuclear cells (systemic acute toxicity)". P_PBMCs were generated from blood obtained from the Red Cross under the authorization LBMCC-2019-0001: "Assessment of differential toxicity of new drugs or drug combinations in preclinical development in ex-vivo proliferating peripheral blood mononuclear cells vs. proliferating cancer cells."

All cell models were maintained at 37 °C in a humid atmosphere with 5 % $CO_2$ in Roswell Park Memorial Institute (RPMI)-1640 medium containing 1 % antibiotics (streptomycin and penicillin) and antimycotics (Lonza, Verviers, Belgium) and 10 % heat-inactivated fetal bovine serum (Lonza).

### 4.2.3. Oxygraphy measurements on K-562 cells

The principle of respirometry in a closed chamber is based on monitoring oxygen consumption concentration, which decreases as the biological sample consumes oxygen [33]. The rate of $O_2$ consumption by $10^6$ K-562 cells was monitored in 2 mL of air-saturated DMEM with polarographic oxygen microelectrodes (Oroboros Oxygraph, Paar, Graz, Austria) at 37 °C. Each compound was added at the final concentration of 10 µM from the stock solution (1 mM, 100x dilution) prepared in DMSO. Twenty microliters of the 1 mM stock solution of cromakalim or DMSO used as a vehicle or benzopyrans (BPDZ 711, BPDZ 811, and BPDZ 812) were added to the cell (1x$10^6$ cells) suspension about 10 min after the start of the cellular respiration (closing the chamber, 2 mL of total volume). Each experiment was performed independently in triplicate, unless otherwise indicated.

To evaluate the compounds' effects on mitochondrial parameters, the experiment was conducted in the presence of substrates (1 µL of oligomycin 2.5 µM, and successive additions of 2 µL of FCCP 1 µM until reaching maximal respiration) and inhibitors (1 µL of rotenone 0.5 µM and 1 µL of antimycin A 1 µM).

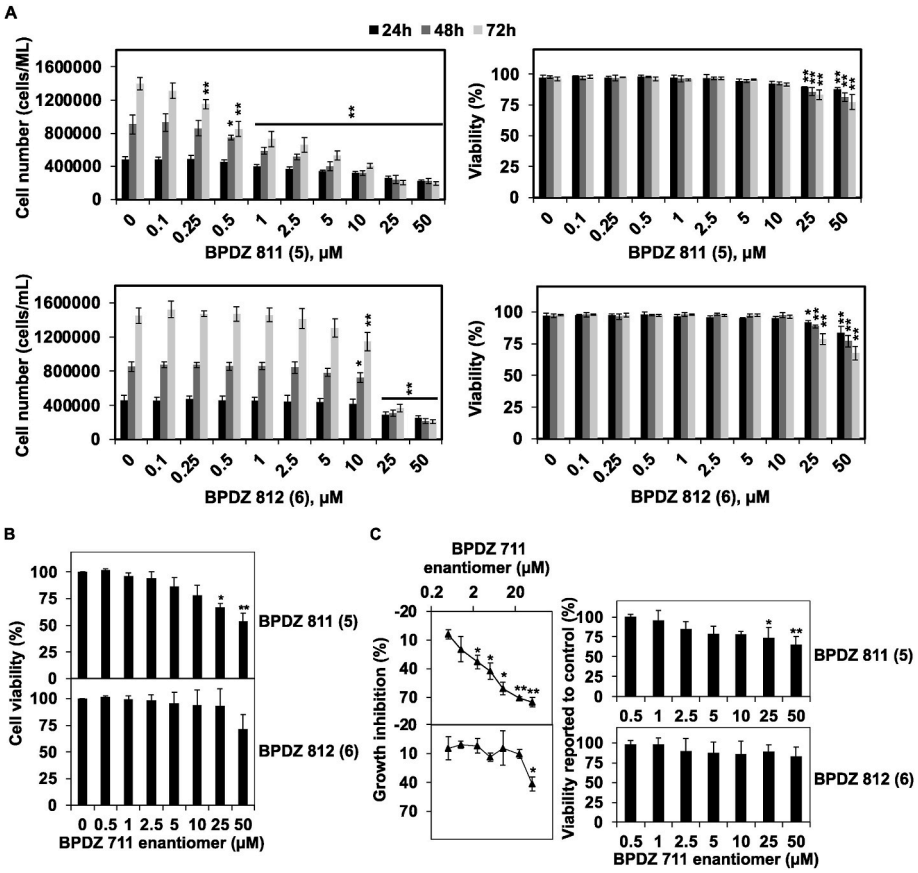


**Fig. 13.** Effect of BPDZ 711 enantiomers on the proliferation and viability of chronic myeloid leukemia and healthy cells. K-562 chronic myeloid leukemia cells (**A**) and non-proliferating (**B**) or proliferating (**C**) peripheral blood mononuclear cells from healthy donors were treated with increasing concentrations of the indicated BPDZ 711 enantiomers. After 72h of incubation or the indicated time points, cell proliferation and viability were assessed using the Trypan blue exclusion test. Data represent the mean ± SD of three independent experiments. P values were calculated by one-way ANOVA with Dunnett's multiple comparison test. * and ** indicate $P < 0.05$ and $P < 0.01$, respectively, versus control cells.

**Table 3**
Effect of BPDZ 711 (4) and its enantiomers BPDZ 811 (5, R-BPDZ 711) and BPDZ 812 (6, S-BPDZ 711) on leukemia cells.
K-562 chronic myeloid leukemia cells were treated with a range of concentrations of the indicated compound, and the proliferation was evaluated by Trypan Blue exclusion assay after 72h of incubation (see Fig. 13A for details).

| Time (h) | $GI_{50}$ (µM)[a] | | |
|---|---|---|---|
| | BPDZ 711 (4)[b] | BPDZ 811 (5) | BPDZ 812 (6) |
| 24 | 5.0 ± 0.7 | 4.3 ± 0.9 | 23.3 ± 1.8 |
| 48 | 2.5 ± 0.4 | 1.4 ± 0.3 | 15.7 ± 2.3 |
| 72 | 1.3 ± 0.1 | 0.9 ± 0.1 | 14.7 ± 1.0 |

[a] $GI_{50}$: drug concentration responsible for inhibiting 50 % of the cell growth (mean ± SD of 3 independent experiments). $GI_{50}$ values were calculated from the inhibitory dose–response curves using the control set to 0 %.
[b] Data obtained in the same experimental conditions and published in Ref. [9].

### 4.2.4. *In vitro HDAC activity assay*

Sirtuin 1-3 activity assays were carried out as previously described [34].

### 4.2.5. *Protein extraction and western blotting*

All the procedures were performed as described in Ref. [7].

### 4.2.6. *Extracellular pH determination*

The pH of the cell culture media was measured using a Cyberscan 500 pH meter (ThermoFisher Scientific, Erembodegem-Aalst, Belgium) equipped with a pH electrode (ThermoFisher Scientific).

**Table 4**
Effect of BPDZ 711 (4) and its enantiomers BPDZ 811 (5, R-BPDZ 711) and BPDZ 711 (6, S-BPDZ 812) on healthy cells.
Proliferating peripheral blood mononuclear cells from healthy donors were treated with a range of concentrations of the indicated compounds, and the proliferation and viability were evaluated by Trypan Blue exclusion assay after 72h of incubation (see Fig. 13C for details).

| Compound | $GI_{50}$ (µM)[a] | $LD_{50}$ (µM)[b] | Selectivity factor for cancer cells[c] |
|---|---|---|---|
| BPDZ 711 (**4**)[d] | 16.6 ± 4.4 | >50 | 12.8 ± 0.3 |
| BPDZ 811 (**5**) | 7.2 ± 1.0 | >50 | 8.0 ± 0.8 |
| BPDZ 812 (**6**) | >50 | >50 | N.A. |

[a] $GI_{50}$: drug concentration responsible for inhibiting 50 % of the cell growth (mean ± SD of 3 independent experiments). GI50 values were calculated from the inhibitory dose–response curves using the control set to 0 %.
[b] LD50: drug concentration responsible for the induction of 50 % of cell death (mean ± SD of 3 independent experiments).
[c] Selectivity factor as the ratio $GI_{50}$(healhy)/$GI_{50}$(CML).
[d] Data obtained in the same experimental conditions and published in Ref. [9].
N.A.: not applicable.

### 4.2.7. *Cell viability and proliferation test*

Cell concentration and viability were measured using an automated image-based cell analyzer (LUNA-FX7TM; Logos Biosystems, Westburg Life Sciences) based on Trypan blue exclusion staining (Roche). The percentage of cell growth inhibition (GI) was determined using the formula: $[(C_n - C_0) - (T_n - T_0)]/(C_n - C_0) \times 100$ where $C_0$, $C_n$, $T_0$, and $T_n$ represent the number of control (C) or treated (T) cells/mL at time 0 and

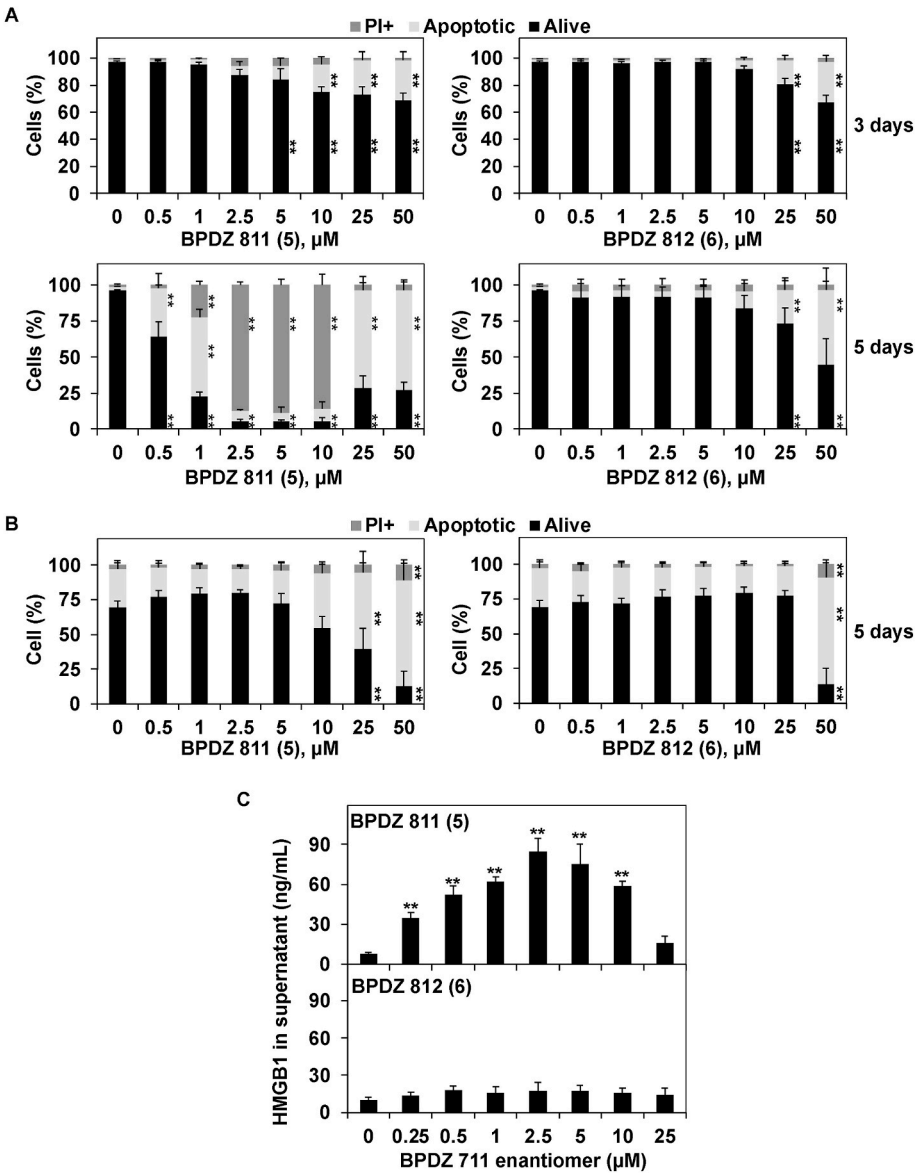


**Fig. 14.** Effect of BPDZ 711 enantiomers on cell death. K-562 chronic myeloid leukemia cells (**A, C**) and proliferating peripheral blood mononuclear cells from healthy donors (**B**) were treated with increasing concentrations of the indicated BPDZ 711 enantiomers. (**A, B**) Quantification of apoptotic, PI-positive and living cell populations based on nuclear morphology analyses after the indicated time of treatment. (**C**) Quantification of HMGB1 release in the cell culture supernatant after 4 days of incubation. Data represent the mean ± SD of three independent experiments. P values were calculated by one-way ANOVA with Dunnett's multiple comparison test. * and ** indicate $P < 0.05$ and $P < 0.01$, respectively, versus control cells.

time n, respectively.

#### *4.2.8. Analysis of nuclear morphology by fluorescence microscopy*

Nuclear morphology analyses were performed as previously described [35].

#### *4.2.9. Quantification of HMGB1 in supernatants*

The release of HMGB1 in the cell culture supernatants was quantified using an HMGB1 ELISA kit (TECAN, IBL, Gent, Belgium) following the manufacturer's instructions.

#### *4.2.10. Statistical analysis and additional analyses*

Statistical analyses were performed using Prism software (v10.2.3). The significance threshold for P values was set below 0.05.

Reported viability and GI values were used to determine the concentration of the drug responsible for the inhibition of 50 % ($IC_{50}$) of the viability and proliferation, namely lethal dose 50 ($LD_{50}$) and $GI_{50}$, respectively, using a log(inhibitor) vs. normalized response nonlinear regression performed with the Prism software.

## CRediT authorship contribution statement

**Michael Schnekenburger:** Writing – review & editing, Supervision, Methodology, Investigation, Funding acquisition. **Eric Goffin:** Writing – review & editing, Methodology, Investigation. **Matthieu Schoumacher:** Methodology, Investigation. **Nikolay Tumanov:** Methodology, Investigation. **Ange Mouithys-Mickalad:** Writing – review & editing, Methodology, Investigation, Conceptualization. **Pascal de Tullio:** Writing – review & editing, Methodology, Investigation, Conceptualization. **Johan Wouters:** Writing – review & editing, Methodology, Investigation. **Philippe Lebrun:** Writing – review & editing, Supervision, Methodology, Investigation, Conceptualization. **Marc Diederich:** Writing – review & editing, Supervision, Methodology, Investigation, Funding acquisition, Conceptualization. **Bernard Pirotte:**

**Table 5**
Effect of BPDZ 711 (4) and its enantiomers BPDZ 811 (5, R-BPDZ 711) and BPDZ 812 (6, S-BPDZ 711) on cell death.
K-562 chronic myeloid leukemia cell line and proliferating peripheral blood mononuclear cells (P_PBMCs) from healthy donors were treated with a range of concentrations of the indicated compounds. After 5 days of incubation, the proportion of cell death was determined by nuclear morphology analyses (see Fig. 14A and B for details).

| Compound | K-562,$LD_{50}$ (μM)[a] | P_PBMC, $LD_{50}$ (μM)[a] | Selectivity factor for cancer cells[b] |
|---|---|---|---|
| BPDZ 711 (**4**)[c] | 2.7 ± 0.7 | 58.0 ± 3.9 | 21.2 ± 0.2 |
| BPDZ 811 (**5**) | 1.4 ± 0.2 | 27.6 ± 7.7 | 19.9 ± 0.3 |
| BPDZ 812 (**6**) | 54.0 ± 9.5 | 42.2 ± 11.1 | 0.8 ± 0.3 |

[a] $LD_{50}$: drug concentration responsible for the induction of 50 % of cell death (mean ± SD of 3 independent experiments).
[b] Selectivity factor as the ratio $GI_{50}$(healthy)/$GI_{50}$(CML).
[c] Data obtained in the same experimental conditions and published in Ref. [9].

Writing – original draft, Supervision, Resources, Project administration, Methodology, Investigation, Conceptualization.

## Declaration of competing interest

The authors declare that they have no known competing financial interests or personal relationships that could have appeared to influence the work reported in this paper.

## Acknowledgments

This study was partly supported by a grant from the National Fund for Scientific Research (FNRS, Belgium) of which P. de Tullio is a Research Director. S. Counerotte and F. Leleux's technical assistance is gratefully acknowledged. MS and MD thank the "Recherche Cancer et Sang" foundation, the "Recherches Scientifiques Luxembourg" organization, the "Een Häerz fir kriibskrank Kanner" organization, the Action LIONS "Vaincre le Cancer" organization, and Télévie Luxembourg for funding. MD also thanks the National Research Foundation (NRF) (Grant Number 370C-20220063); MEST of Korea for Tumor Microenvironment Global Core Research Center (GCRC) (Grant Number 2011-0030001); Brain Korea (BK21) PLUS program and Creative-Pioneering Researchers Program at Seoul National University (Funding number: 370C-20160062).

## Appendix A. Supplementary data

Supplementary data to this article can be found online at https://doi.org/10.1016/j.ejmcr.2024.100244.

## Data availability

Data will be made available on request.

## References

[1] S. Sebille, D. Gall, P. de Tullio, X. Florence, P. Lebrun, B. Pirotte, Design, synthesis, and pharmacological evaluation of R/S-3,4-dihydro-2,2-dimethyl-6-halo-4-(phenylaminocarbonylamino)-2*H*-1-benzopyrans: toward tissue-selective pancreatic beta-cell $K_{ATP}$ channel openers structurally related to (+/-)-cromakalim, J. Med. Chem. 49 (2006) 4690–4697, https://doi.org/10.1021/jm060161z.
[2] S. Sebille, P. de Tullio, X. Florence, B. Becker, M.-H. Antoine, C. Michaux, J. Wouters, B. Pirotte, P. Lebrun, New R/S-3,4-dihydro-2,2-dimethyl-6-halo-4-(phenylaminothiocarbonylamino)-2*H*-1-benzopyrans structurally related to (+/-)-cromakalim as tissue-selective pancreatic beta-cell $K_{ATP}$ channel openers, Bioorg. Med. Chem. 16 (2008) 5704–5719, https://doi.org/10.1016/j.bmc.2008.03.065.
[3] X. Florence, S. Sebille, P. de Tullio, P. Lebrun, B. Pirotte, New R/S-3,4-dihydro-2,2-dimethyl-2*H*-1-benzopyrans as $K_{ATP}$ channel openers: modulation of the 4-position, Bioorg. Med. Chem. 17 (2009) 7723–7731, https://doi.org/10.1016/j.bmc.2009.09.041.
[4] X. Florence, S. Dilly, P. de Tullio, B. Pirotte, P. Lebrun, Modulation of the 6-position of benzopyran derivatives and inhibitory effects on the insulin releasing process, Bioorg. Med. Chem. 19 (2011) 3919–3928, https://doi.org/10.1016/j.bmc.2011.05.040.
[5] B. Pirotte, X. Florence, E. Goffin, M.B. Medeiros, P. de Tullio, P. Lebrun, 4-Phenylureido/thioureido-substituted 2,2-dimethylchroman analogs of cromakalim bearing a bulky 'carbamate' moiety at the 6-position as potent inhibitors of glucose-sensitive insulin secretion, Eur. J. Med. Chem. 121 (2016) 338–351, https://doi.org/10.1016/j.ejmech.2016.05.042.
[6] E. Goffin, D. Lamoral-Theys, N. Tajeddine, P. de Tullio, L. Mondin, F. Lefranc, P. Gailly, B. Rogister, R. Kiss, B. Pirotte, N-Aryl-N'-(chroman-4-yl)ureas and thioureas display in vitro anticancer activity and selectivity on apoptosis-resistant glioblastoma cells: screening, synthesis of simplified derivatives, and structure-activity relationship analysis, Eur. J. Med. Chem. 54 (2012) 834–844, https://doi.org/10.1016/j.ejmech.2012.06.050.
[7] M. Schnekenburger, E. Goffin, J.Y. Lee, J.Y. Jang, A. Mazumder, S. Ji, B. Rogister, N. Bouider, F. Lefranc, W. Miklos, V. Mathieu, P. de Tullio, K.W. Kim, M. Dicato, W. Berger, B.W. Han, R. Kiss, B. Pirotte, M. Diederich, Discovery and characterization of R/S-N-3-cyanophenyl-N'-(6-tert-butoxycarbonylamino-3,4-dihydro-2,2-dimethyl-2*H*-1-benzopyran-4-yl)urea, a new histone deacetylase class III inhibitor exerting antiproliferative activity against cancer cell lines, J. Med. Chem. 60 (2017) 4714–4733, https://doi.org/10.1021/acs.jmedchem.7b00533.
[8] A. Mouithys-Mickalad, J. Ceusters, M. Charif, B. El Moualij, M. Schoumacher, S. Plyte, T. Franck, L. Bettendorff, B. Pirotte, D. Serteyn, P. de Tullio, Modulation of mitochondrial respiration rate and calcium-induced swelling by new cromakalim analogues, Chem. Biol. Interact. 331 (2020) 109272, https://doi.org/10.1016/j.cbi.2020.109272.
[9] M. Schnekenburger, A. Lorant, S.R. Gajulapalli, R. Rajora, J.Y. Lee, A. Mazumder, H. Yang, C. Christov, H.J. Kang, B. Pirotte, M. Diederich, Dual inhibition of sirtuins 1 and 2: reprogramming metabolic energy dynamics in chronic myeloid leukemia as an immunogenic anticancer strategy, Cancer Commun. 44 (2024) 915–920, https://doi.org/10.1002/cac2.12590.
[10] V.S. Bryantsev, T.K. Firman, B.P. Hay, Conformational analysis and rotational barriers of alkyl- and phenyl-substituted urea derivatives, J. Phys. Chem. A 109 (2005) 832–842, https://doi.org/10.1021/jp0457287.
[11] Dinesh Rajnikant, M.B. Deshmukh, Kamni, Synthesis, X-ray structure and N-H…O interactions in 1,3-diphenyl-urea, Bull. Mater. Sci. 29 (2006) 239–242, https://doi.org/10.1007/BF02706491.
[12] A. Okuniewski, J. Chojnacki, B. Becker, *N,N'*-Diphenylthiourea acetone monosolvate, Acta Cryst E67 (2011) o55, https://doi.org/10.1107/S1600536810050300.
[13] M. Matsumura, A. Tanatani, I. Azumaya, H. Masu, D. Hashizume, H. Kagechika, A. Muranaka, M. Uchiyama, Unusual conformational preference of an aromatic secondary urea: solvent-dependent open-closed conformational switching of N,N-bis(porphyrinyl)urea, Chem. Commun. 49 (2013) 2290, https://doi.org/10.1039/c2cc37583d.
[14] M.A. Solomos, T.A. Watts, J.A. Swift, Ortho-substituent effects on diphenylurea packing motifs, Cryst. Growth Des. 17 (2017) 5065–5072, https://doi.org/10.1021/acs.cgd.7b00757.
[15] L. Chęcińska, W. Morgenroth, C. Paulmann, D. Jayatilaka, B. Dittrich, A comparison of electron density from Hirshfeld-atom refinement, X-ray wavefunction refinement and multipole refinement on three urea derivatives, Cryst. Eng. Commun. 15 (2013) 2084–2090, https://doi.org/10.1039/C2CE26964C.
[16] A.K. Ghosh, M. Brindisi, Urea derivatives in modern drug discovery and medicinal chemistry, J. Med. Chem. 63 (2020) 2751–2788, https://doi.org/10.1021/acs.jmedchem.9b01541.
[17] J.D. Ceusters, A.A. Mouithys-Mickalad, T.J. Franck, S. Derochette, A. Vanderplasschen, G.P. Deby-Dupont, D.A. Serteyn, Effect of myeloperoxidase and anoxia/reoxygenation on mitochondrial respiratory function of cultured primary equine skeletal myoblasts, Mitochondrion 13 (2013) 410–416, https://doi.org/10.1016/j.mito.2012.12.004.
[18] D. Wang, B. Song, X. Zhong, X.-F. Sun, Y. Fan, Phytohaemagglutinin stimulates the proliferation of peripheral blood mononuclear cells and expression of secretory cytokines, Chinese Journal of Tissue Engineering Research 18 (2014) 3707–3714, https://doi.org/10.3969/j.issn.2095-4344.2014.23.017.
[19] P. Scaffidi, T. Misteli, M.E. Bianchi, Release of chromatin protein HMGB1 by necrotic cells triggers inflammation, Nature 418 (2002) 191–195, https://doi.org/10.1038/nature00858.
[20] J.-H. Lee, M.L. Choy, L. Ngo, S.S. Foster, P.A. Marks, Histone deacetylase inhibitor induces DNA damage, which normal but not transformed cells can repair, Proc. Natl. Acad. Sci. U.S.A. 107 (2010) 14639–14644, https://doi.org/10.1073/pnas.1008522107.
[21] Y. Chen, Y.-H. Tsai, S.-H. Tseng, HDAC inhibitors and RECK modulate endoplasmic reticulum stress in tumor cells, Int. J. Mol. Sci. 18 (2017) 258, https://doi.org/10.3390/ijms18020258.
[22] M.J. Slaughter, E.K. Shanle, A. Khan, K.F. Chua, T. Hong, L.D. Boxer, C.D. Allis, S. Z. Josefowicz, B.A. Garcia, S.B. Rothbart, B.D. Strahl, I.J. Davis, HDAC inhibition results in widespread alteration of the histone acetylation landscape and BRD4 targeting to gene bodies, Cell Rep. 34 (2021) 108638, https://doi.org/10.1016/j.celrep.2020.108638.
[23] J.A. Halsall, B.M. Turner, Histone deacetylase inhibitors for cancer therapy: an evolutionarily ancient resistance response may explain their limited success, Bioessays 38 (2016) 1102–1110, https://doi.org/10.1002/bies.201600070.

[24] J. King, M. Patel, S. Chandrasekaran, Metabolism, HDACs, and HDAC inhibitors: a systems biology perspective, Metabolites 11 (2021) 792, https://doi.org/10.3390/metabo11110792.
[25] O. Rigaku, CrysAlis PRO Software System, Rigaku Corporation, Oxford, UK, 2018.
[26] G. Sheldrick, SHELXS-97, Program for Crystal Structure Determination, University of Göttingen, Germany, 1997.
[27] G.M. Sheldrick, SHELXL-97-2, Program for Crystal Structure Refinement, University of Göttingen, Germany, 1997.
[28] O.V. Dolomanov, L.J. Bourhis, R.J. Gildea, J.A.K. Howard, H. Puschmann, OLEX2: a complete structure solution, refinement and analysis program, J. Appl. Cryst. 42 (2009) 339–341, https://doi.org/10.1107/s0021889808042726.
[29] G. Sheldrick, Shelxtl V6. 1 Software Reference Manual, Bruker AXS Inc, Madison, WI, 2009.
[30] S. Hübschle, G.M. Sheldrick, B. Dittrich, ShelXle: a Qt graphical user interface for SHELXL, J. Appl. Cryst. 44 (2011) 1281–1284, https://doi.org/10.1107/S0021889811043202.
[31] G. Scheldrick, SHELXT-integrated space-group and crystals-structure determination, Acta Crystallogr., Sect. A: Found. Adv. 71 (2015) 3–8, https://doi.org/10.1107/S2053273314026370.
[32] M. Schnekenburger, C. Grandjenette, J. Ghelfi, T. Karius, B. Foliguet, M. Dicato, M. Diederich, Sustained exposure to the DNA demethylating agent, 2'-deoxy-5-azacytidine, leads to apoptotic cell death in chronic myeloid leukemia by promoting differentiation, senescence, and autophagy, Biochem. Pharmacol. 81 (2011) 364–378, https://doi.org/10.1016/j.bcp.2010.10.013.
[33] E. Hütter, H. Unterluggauer, A. Garedew, P. Jansen-Dürr, E. Gnaiger, High-resolution respirometry - a modern tool in aging research, Exp. Gerontol. 41 (2006) 103–109, https://doi.org/10.1016/j.exger.2005.09.011.
[34] M. Schnekenburger, V. Mathieu, F. Lefranc, J.Y. Jang, M. Masi, A. Kijjoa, A. Evidente, H.-J. Kim, R. Kiss, M. Dicato, B.W. Han, M. Diederich, The fungal metabolite eurochevalierine, a sequiterpene alkaloid, displays anti-cancer properties through selective Sirtuin 1/2 inhibition, Molecules 23 (2018) 333, https://doi.org/10.3390/molecules23020333.
[35] G. Greco, M. Schnekenburger, E. Catanzaro, E. Turrini, F. Ferrini, P. Sestili, M. Diederich, C. Fimognari, Discovery of sulforaphane as an inducer of ferroptosis in U-937 leukemia cells: expanding its anticancer potential, Cancers 14 (2022) 76, https://doi.org/10.3390/cancers14010076.